# Reconfigurable Multi-Band Microwave Filters

Roberto Gómez-García, *Senior Member, IEEE*, and Andrew C. Guyette, *Member, IEEE*

***Abstract*—An original and simple approach to the design of fully reconfigurable multi-band microwave bandpass filters (BPFs) with an arbitrary number of passbands is reported in this paper. It exploits the use of an innovative quasi-BPF configuration made up of different sets of controllable mono-frequency resonators to separately shape each tunable passband. Thus, high-selectivity multi-band bandpass filtering transfer functions exhibiting independent control in terms of center frequency, bandwidth, and transmission zeros can be synthesized. Furthermore, as an unprecedented frequency-agility feature of the proposed reconfigurable multi-band BPF structure when compared to the state-of-the-art, its passbands can be merged together to form broader, and for certain realizations, higher order transmission bands. This allows even more degrees of reconfiguration to be achieved in the devised circuit, which can also operate as ultra-wideband BPF with flexible in-band notches or self-equalized flat-group-delay quasi-elliptic-type BPF. The theoretical foundations of the described reconfigurable multi-band BPF scheme, along with guidelines for its design and a triple-passband filter synthesis example based on the coupled-node formalism, are expounded. In addition, as an experimental proof-of-concept, two microstrip prototypes with high-$Q$ tuning implemented through mechanically variable capacitors are manufactured and tested. They are a wideband dual-band BPF and a quadruple-band BPF with narrow-bandwidth passbands.**

***Index Terms*—Bandpass filters (BPFs), coupled-resonator filters, microstrip filters, microwave filters, multi-band filters, planar filters, reconfigurable filters, transmission zero (TZ), tunable circuits and devices, ultra-wideband (UWB) technology.**

## I. Introduction

EMERGING applications in the telecommunications and radar sectors require the availability of flexible and multi-purpose microwave circuits as well as systems capable of supporting them. This has relaunched the interest in the field of reconfigurable high-frequency electronics, where a large variety of advanced frequency-agile passive and active devices are being developed (e.g., [1]–[5]). A special effort has been directed towards research into frequency-controllable filtering devices, as they are key components needed to carry out the fully adjustable signal-band selection or interference suppression processes required by modern RF front-ends. Specifically, reconfigurable multi-band bandpass filters (BPFs) are highly desired in multi-mode transceiver architectures for multi-standard wireless communications. High-speed tunable wideband multi-notch and multi-stopband filters capable of simultaneously mitigating multiple jamming signals in a dynamic fashion are also in very high demand in ultra-broadband receivers, which sense large portions of the spectrum, such as in software-defined radio (SDR) and electronic warfare support measure (ESM) scenarios [6], [7].

Over the years, tunable BPF design techniques have become well established for mono-band filters. A plurality of solutions have been suggested to properly control the center frequency in single-band BPFs for hybrid and 3-D technologies by inserting variable-reactance elements into a filter's resonators; for instance, p-i-n, Schottky, varactor diodes, ferroelectric barium–strontium–titanate (BST) capacitors, or microelectromechanical systems (MEMS) when power-handling capability and linearity are an issue [8]–[11]. Less-mature approaches based on altering the substrate effective dielectric permittivity in planar BPFs by means of piezoelectric and liquid-crystal methods have also been devised [12], [13]. More recently, procedures to tune the bandwidth and even the transmission zeros (TZs) in BPFs have been shown, leading to higher levels of reconfiguration for these devices. They rely on very different mechanisms, such as the modification of the electromagnetic couplings between resonators in coupled-resonator BPFs, the generation of controllable interactions in signal-interference BPFs, and the aggregation of narrower passbands in switchable contiguous-channel filters [14]–[20]. Other trends in the tunable BPF area focus on the realization of filtering components with selectable functionality between different states, such as the bandpass and bandstop type [21].

In contrast, as a more challenging design goal, few practical realizations of reconfigurable multi-band BPFs have been proposed to date despite their increasing importance. Furthermore, the reported topologies present some constraints regarding the maximum number of controllable passbands that can be synthesized in their transfer functions (generally no more than two) or their limited tuning capability [22]–[30]. For example, in [22], a low-order recursive-type dual-band active BPF with independently adjustable center frequencies was shown. Drawbacks include a very narrow tuning range, degraded selectivity, and poor insertion-loss performance with the electronic-reconfiguration approach. A varactor-tuned double-band coupled-resonator BPF with separated center-frequency control for passbands was also reported in [23]. This circuit, although demonstrating higher selectivity than that of [22], shares its shortcoming concerning the moderate center-frequency tuning ability for the dual bands

Manuscript received August 19, 2014; revised January 14, 2015 and February 11, 2015; accepted February 13, 2015. The work of R. Gómez-García was supported by the Defense Advanced Research Project Agency (DARPA) and by the Office of Naval Research Global (ONRG) Research Grant N62902-14-1-025 under the Naval International Cooperative Opportunities (NICOP) program.

R. Gómez-García is with the Department of Signal Theory and Communications, University of Alcalá, Alcalá de Henares, 28871 Madrid, Spain (e-mail: roberto.gomez.garcia@ieee.org).

A. C. Guyette is with Code 6851, Naval Research Laboratory, Washington, DC 20375-5347 USA (e-mail: andrew.guyette@nrl.navy.mil).

Color versions of one or more of the figures in this paper are available online at http://ieeexplore.ieee.org.

Digital Object Identifier 10.1109/TMTT.2015.2405066

when one of them remains fixed. This is also the case of the more-compact double-band BPF transversal topology of [24], which is shaped by multi-stub-loaded resonators with variable interactions through varactors. In [25]–[28], four approaches of two-band BPFs with reconfigurable passbands in terms of both center frequency and bandwidth were detailed. These configurations, although well-suited for dual-band designs since they are made up of dual-mode resonators, can hardly be extrapolated to multi-band BPFs with more than two bands. Finally, a reconfigurable quasi-elliptic-type triple-band BPF based on a defected-ground structure (DGS) was proposed in [29]. It incorporates, as basic frequency-agility feature, the on/off electronic switching of three passbands through diodes to configure single-, dual-, and triple-band filtering states. Such multi-channel commutation functionality, among others, can be implemented for any number of transmission bands by using intrinsically switchable filter banks, as verified in [30].

On the other hand, the development of flexible bandstop and notch filters with frequency tuning throughout ultra-broad transmission ranges is also of great interest [31], [32]. Moreover, some approaches that integrate this dynamic bandstop/notch filtering action in UWB BPFs have been conceived, aimed at realizing broad spectrum bands free of in-band interference/jamming signals [33]–[35]. These techniques have been validated in experimental BPF circuits with no more than two adjustable in-band notches and lacking of reconfiguration capability for the overall passband.

A new class of fully reconfigurable multi-band microwave BPFs is reported in this paper. It makes use of an original quasi-BPF topology incorporating multiple sets of tunable resonators to independently configure each passband. The proposed frequency-agile multi-band BPF solution, which exhibits the highest reconfiguration capability demonstrated to date for controllable multi-band microwave BPFs to the best of the authors' knowledge, has the following advantages.

- It is capable of realizing an arbitrary number of passbands in its multi-band transfer function, while enabling an independent tuning for all of them in terms of both center frequency and bandwidth. "Independent tuning" refers here to the possibility to control the electrical characteristics of one passband whereas the others remain nearly static, despite several capacitors (apart from those associated to the tuned passband) could need to be readjusted for it in some specific implementations of this filter approach.
- TZs can be produced at both sides of all its passbands. As a result, high-selectivity multi-band bandpass-filtering functions with sharp-rejection capability can be generated for some reconfiguration states by closely allocating these TZs to the transmission bands.
- In addition to the aforementioned inter-band TZ creation for deep stopband rejection in multi-band responses, the passbands can be merged together to shape broader and for certain realizations higher order transmission bands. Therefore, maximum-bandwidth limitations of classic coupled-resonator BPF schemes made up of single-mode resonators can be overcome through this filter architecture due to this multi-passband aggregation capability.

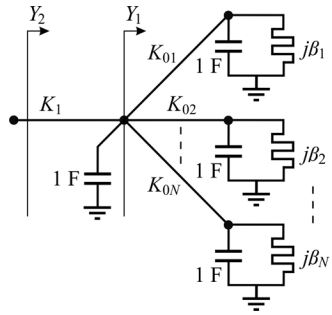


Fig. 1. Low-pass prototype of the quasi-bandpass section.

- Reconfiguration states other than the multi-passband one can be attained in the same circuit; e.g., among them, tune-all wideband bandpass filtering with embedded in-band adaptive notches or self-equalized quasi-elliptic-type bandpass filtering with flat group-delay characteristics.
- Its operation philosophy is suitable for multiple technologies and tunable-resonator geometries.

The remainder of this paper is organized as follows. The theoretical principles of the devised reconfigurable multi-band microwave BPF are presented in Section II. Section III describes the experimental results of two mechanically tunable proof-of-concept prototypes developed in microstrip substrate with dual- and quadruple-band responses. Finally, a summary and the most relevant conclusions of this work are given in Section IV.

## II. Theoretical Foundations

The proposed reconfigurable multi-band microwave BPF approach is based on an original class of multi-resonance building block called a "quasi-bandpass" section. Here, the theoretical foundations of the quasi-bandpass section are expounded. After that, information about how this constitutive filtering network can be employed for higher order quasi-BPF design is provided. Furthermore, frequency tuning characteristics of these filters when compared to those of traditional tunable filter topologies are also described. To support the discussion, a synthesis example of a triple-band BPF based on the quasi-bandpass section is also detailed.

### A. Analysis of the Quasi-Bandpass Section

The quasi-bandpass section is the basic building block for the engineered reconfigurable multi-band BPF configuration.

Shown in Fig. 1 is the low-pass prototype of the quasi-bandpass section. It is a one-port network comprised of $N$ resonators (referred to here as "bandpass" resonators) coupled to a single resonator (referred to here as a "bandstop" resonator), which in turn is coupled to the input. The bandpass resonators are coupled to the bandstop resonator with couplings $K_{0k}$, and the frequency offsets are represented by susceptances $\beta_k$ ($k = 1, 2, \ldots, N$). The bandstop resonator is coupled to the input with inverter $K_1$. With reference to Fig. 1, the admittance $Y_1$ looking into the network of coupled bandpass resonators is given by ($p = j\omega$ is the complex frequency variable)

$$Y_1 = \sum_{k=1}^{N} \frac{K_{0k}^2}{p + j\beta_k}. \tag{1}$$

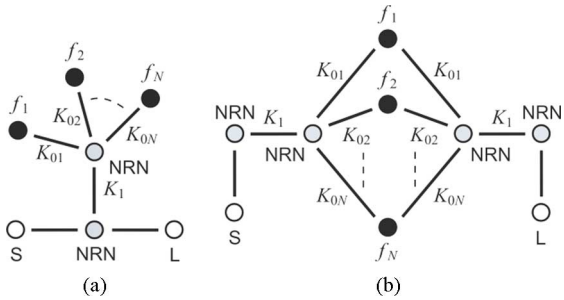


Fig. 2. Narrowband approximation of the quasi-bandpass section and equivalent transversally coupled resonator network (white circles: source (S) and load (L); black circles: resonating nodes; grey circles: non-resonating nodes (NRNs); black lines: couplings). (a) Approximation. (b) Equivalent transversal network.

The input admittance $Y_2$ of the quasi-bandpass section, assuming small values of $p$ (i.e., close to the resonant frequency of the bandstop resonator), is

$$Y_2 = \frac{K_1^2}{p + Y_1} \cong \frac{K_1^2}{Y_1}. \tag{2}$$

The simplified narrowband approximation of a quasi-bandpass section is shown in Fig. 2(a), where the bandstop resonator of Fig. 1 has been replaced with a non-resonating node (NRN) with zero susceptance. Using even/odd-mode analysis it can be readily shown that this circuit is equivalent to the transversally coupled resonator network of Fig. 2(b) [36].

It is instructive to compare Fig. 2(b) to the transversally coupled resonator network of a conventional filter function [37] (e.g., Chebyshev), where transversal resonator networks adjacent in resonant frequency have a 180° phase difference between them in order to achieve constructive interference and form a single passband. In contrast, because all couplings are of the same sign, destructive rather than constructive interference occurs between resonances. Therefore, this network is capable of generating $N$ first-order bandpass responses with real-frequency TZs appearing between these bands.

### *B. Higher Order Quasi-BPFs*

Higher order bandpass responses can be realized by simply cascading identically tuned quasi-bandpass sections, as shown in Fig. 3(a). From a practical design perspective, the effects of other passbands on a given passband can be ignored (i.e., other transversal resonator sections of Fig. 3(a) appear as open circuits). Shown in Fig. 3(b) is the general multi-band quasi-bandpass response. Note that the stopband bandwidth (that is the operational bandwidth of the quasi-bandpass response) is determined by the bandwidth of the stopband created by the bandstop resonators.

In the topology of Fig. 3(a), adjacent passbands remain separated by TZs, and cannot be merged together to form a single higher order and broader bandpass response. In order to allow multiple bands to combine to form a continuous passband, multiple quasi-bandpass networks can be placed in a transversal configuration, where at least one network is 180° out-of-phase with the others. This is exemplified in Fig. 4 for a two-path transversal implementation of the quad-band BPF enabling passband merging among its four second-order transmission bands. Note that, unlike in Fig. 3(a) and as another

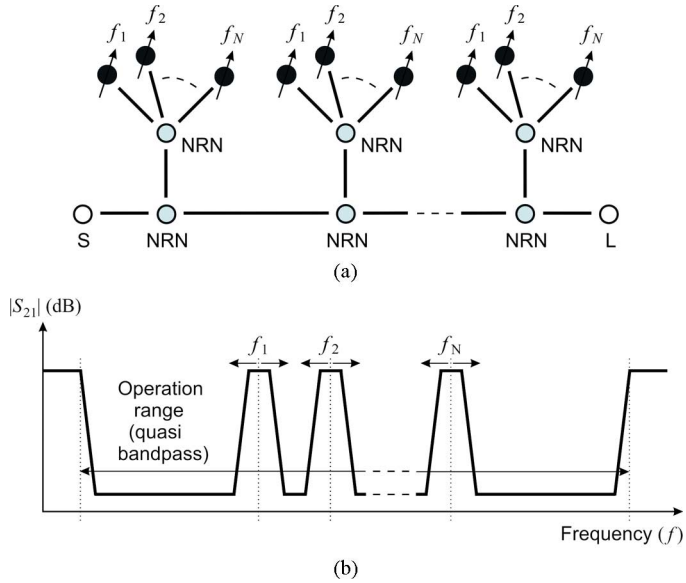


Fig. 3. Coupling structure and principle of the proposed reconfigurable multi-band BPF concept based on the quasi-BPF approach. (a) Coupling structure (white circles: source (S) and load (L); black circles: resonating nodes; grey circles: non-resonating nodes (NRNs); black lines: couplings). (b) Principle of operation.

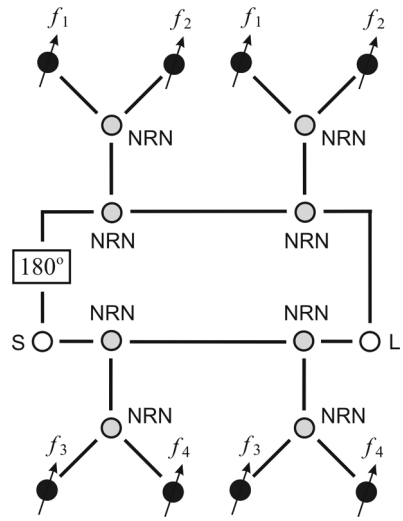


Fig. 4. Coupling structure of an example of two-path transversal reconfigurable quad-band BPF with passband merging based on the quasi-BPF approach (white circles: source (S) and load (L); black circles: resonating nodes; grey circles: non-resonating nodes (NRNs); black lines: couplings).

alternative for the realization of the multi-band BPF, not all the resonators associated to different bands need to be coupled to the same NRN. That is, not all the quasi-bandpass sections must resonate for the $N$ passbands to be shaped. Thus, a different quasi-bandpass stage can be utilized as building block of each transversal branch of the overall filter to synthesize a higher number of transmission bands.

### *C. Frequency Tuning Characteristics of Quasi-BPFs*

In addition to straightforwardly generating multiple passbands, the quasi-bandpass topology also has a clear advantage when it comes to the realization of tunable responses over conventional filter topologies. In a conventional tunable filter, resonators are either coupled to each other or to the input/output ports, and so the tuned center-frequency dependence of the

couplings is difficult to make uniform throughout the filter. This results in degradation of the transfer function with tuning. This can be especially problematic when the inter-resonator couplings are a mix of electric and magnetic (used, for example, to control the bandwidth versus tuned center frequency profile as needed in constant absolute-bandwidth frequency-adjustable BPFs).

In a quasi-BPF, all of the bandpass resonators are coupled only once to identical NRNs, allowing all couplings to be easily designed to have identical tuned-frequency dependence. The resonator-to-NRN coupling can therefore be engineered to give desired bandwidth versus tuned center frequency profile, and the filter will naturally be matched across the entire tuning range, provided of course the tuning range falls within the operational range of the quasi-bandpass response.

### *D. Synthesis Example*

As a supporting theoretical example, this section describes the synthesis of a triple-band BPF using the narrowband-approximation quasi-bandpass section of Fig. 2 and following the coupling-node formalism. This is done to corroborate the theoretical suitability of this quasi-bandpass network for multi-band BPF design from which physical microwave planar realizations can be properly derived from conventional filter implementation techniques. A multi-band frequency transformation compatible with the engineered quasi-bandpass topology of Fig. 2 is given by

$$\Omega = \frac{1}{\sum_{k=1}^{N} \frac{1}{\alpha_k \left( \frac{\omega}{\omega_k} - \frac{\omega_k}{\omega} \right)}} \tag{3}$$

where $\omega$ is frequency in radians, $\omega_k$ is the center frequency in radians of the $k$th band, $\alpha_k$ is the bandwidth scaling factor of the $k$th band, and $N$ is the number of bands.

Fig. 5 illustrates the application of this multi-band transformation to a single low-pass prototype resonator. The input admittance of the low-pass prototype resonator [see Fig. 5(a)] is

$$Y_{\text{in}}(j\omega) = j\omega. \tag{4}$$

The input admittance of the transformed network is then

$$Y_{\text{in}}(j\omega)|_{\omega \to \Omega} = \frac{1}{\sum_{k=1}^{N} \frac{1}{j\alpha_k \left( \frac{\omega}{\omega_k} - \frac{\omega_k}{\omega} \right)}}. \tag{5}$$

This admittance has the same general form as (2), and so it can be readily realized using a quasi-bandpass section [see Fig. 5(b)]. The resonators $R_k$ ($k = 1, 2, \ldots, N$) are parallel lumped-element resonators with inductor ($L_k$) and capacitor ($C_k$) element values given by

$$L_k = \frac{1}{\alpha_k \omega_k}(H) \tag{6}$$

$$C_k = \frac{\alpha_k}{\omega_k}(F). \tag{7}$$

Fig. 6 shows a normalized low-pass prototype giving a third-order Chebyshev response with 20-dB return-loss ripple. This network was synthesized using conventional techniques [37].

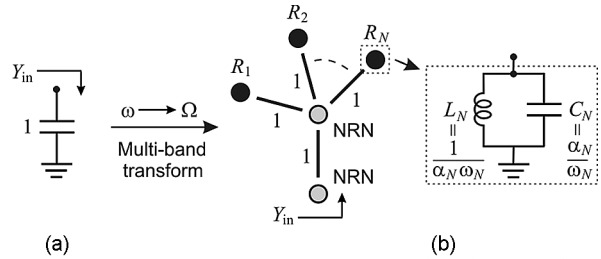


Fig. 5. (a) Normalized low-pass prototype resonator. (b) Prototype resonator after application of the multi-band frequency transformation (4).

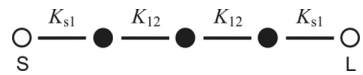


Fig. 6. Third-order Chebyshev low-pass prototype ($K_{s1} = 1.0825$ and $K_{12} = 1.0303$).

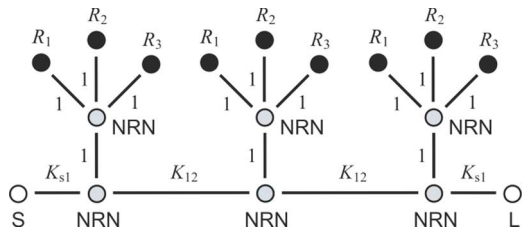


Fig. 7. Third-order triple-band bandpass prototype network.

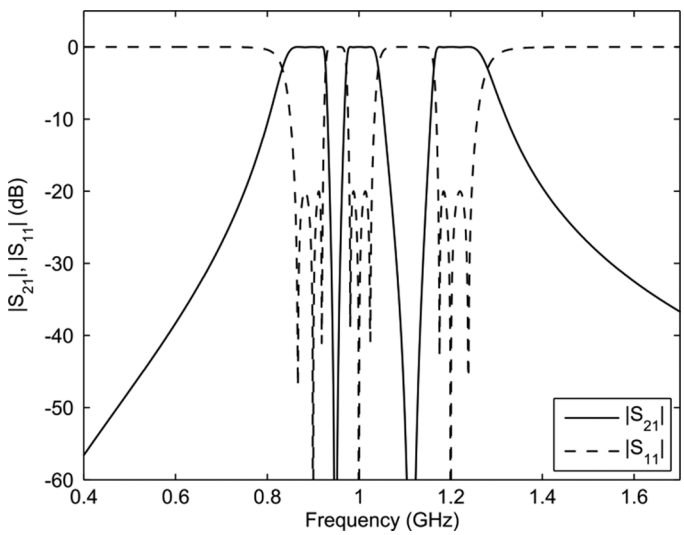


Fig. 8. Power transmission ($|S_{21}|$) and reflection ($|S_{11}|$) responses of the ideal synthesized third-order triple-band bandpass network shown in Fig. 7.

The multi-band transformation (3) is then applied with values (note that $\omega_k = 2\pi f_k$).

- First passband: $\alpha_1 = 15$ and $f_1 = 0.9$ GHz.
- Second passband: $\alpha_2 = 19$ and $f_2 = 1$ GHz.
- Third passband: $\alpha_3 = 17$ and $f_3 = 1.2$ GHz.

The resulting prototype multi-band network is shown in Fig. 7. The elements values of the resonators $R_1$, $R_2$, and $R_3$ are calculated using (6) and (7).

- First passband: $L_1 = 11.79$ pH and $C_1 = 2.653$ nF.
- Second passband: $L_2 = 8.37$ pH and $C_2 = 3.023$ nF.
- Third passband: $L_3 = 7.8$ pH and $C_3 = 2.254$ nF.

Fig. 8 depicts the power transmission and reflection responses of the ideal synthesized third-order triple-band BPF network of Fig. 7. As can be seen, the prefixed passband allocation and in-band ripple-level specifications are fulfilled.

For its physical realization and starting from this ideal synthesized network, the next step in the design process is admittance scaling—first to 50 Ω (or other) input/output impedance, followed by appropriate nodal admittance scaling [36]. The final step is to realize the couplings and resonators in a desired technology using the usual filter implementation techniques, depending on the selected physical structure [38]. Reconfiguration capability can be easily incorporated into the multi-band BPF by adding variable-reactance elements to it. In Section III, two different planar prototypes of fully reconfigurable wideband dual-band and narrowband quad-band BPFs exploiting distinct topologies are described.

## III. Experimental Results

To confirm the experimental viability of the engineered reconfigurable multi-band BPF concept, two multi-stage hybrid prototypes have been designed in a microstrip substrate, fabricated, and measured. They are a third-order broadband dual-band BPF and a quadruple-band BPF with narrow-bandwidth two-pole passbands and tune-all capability. Regarding the construction and characterization processes of these filters, the following issues should be taken into account.

- The prototypes were simulated and optimized with the parametric circuit simulator AWR Microwave Office and the 2.5-D electromagnetic-field simulator SONNET. Thus, the values for the physical dimensions and capacitor variation ranges leading to the required performances for these filters depending on their geometries were extracted. Specifically, their circuit models were initially derived by means of AWR Microwave Office, to be subsequently laid out and simulated through SONNET. Mixed simulations using the scattering parameters of the microstrip structures imported from SONNET into AWR Microwave Office, along with the variable lumped capacitors for tuning, were finally performed.
- For circuit development, a microstrip substrate Rogers RO4003 was selected. Its main parameter values are: relative dielectric permittivity $\varepsilon_r = 3.38$, dielectric thickness $h = 1.52$ mm, metal thickness $t = 17.8$ $\mu$m, and dielectric loss tangent $\tan\delta_D = 0.0027$.
- Mechanically adjustable thin-trim trimmer capacitors from Johanson Manufacturing were used as variable-reactance elements to implement the high-$Q$ tuning. They have the following electrical characteristics: frequency operation up to 2 GHz, measured $Q$ at 100 MHz higher than 500 or 1000 depending on the capacitance variation range, maximum working voltage of 250 V (dc), insulation resistance higher than 10 000 MΩ, and operational temperature range from $-55$ °C to $+125$ °C. As a result, high power-handling capability limited by the breakdown voltage of the trimmer capacitors is conferred to the built filter prototypes, whereas the $Q$ of the overall tunable resonator is mainly determined by the microstrip line.
- An LPKF S62-model mechanical milling machine was employed to mill the circuit patterns, whereas an LPKF *ProConduct* silver epoxy paste was utilized to metallize the via-holes associated to the ground connections. All the surface-mount components were attached to the substrate with EPO-TEK silver epoxy.
- Measurements were taken using an Agilent PNA-X 50-GHz network analyzer and include the effects of the SMA-type input/output connectors.

The results obtained in the simulation and testing of these reconfigurable multi-band BPF prototypes are reported below.

### A. Prototype 1: Wideband Dual-Band BPF

The first prototype is a frequency-agile wideband dual-band BPF with reconfigurable passbands within the one-octave-width spectral range of 0.6–1.2 GHz. It is made up of three identical stages inter-connected through cascading lines. These stages present two different resonators, both formed by a transmission-line segment terminated with a short-circuited variable lumped capacitor. Thus, following the principle of Fig. 3, each stage contributes to each passband with one pole. Note that higher order multi-band BPF realizations can be accomplished by cascading more quasi-bandpass stages, but at the expense of increased design complexity, due to the higher difficulty of attaining reasonable in-band power matching levels for all the passbands and reconfiguration states. In such a case, the exploitation of transversal arrangements, as done in the second prototype of this work, could be a preferred choice.

The layout and a photograph of the built circuit are shown in Fig. 9. Nonredundant physical dimensions are also indicated. As can be seen, to realize the NRNs and the inter-node connecting elements of the stages, transmission-line segments were used. This was done to create strong signal interactions between nodes so that wideband passbands can be generated. In fact, each stage can be viewed as a detuned branch-line coupler (at 1.7 GHz in this case) with tunable resonators attached to its coupled and isolated nodes, respectively, whereas its input and direct ports are taken as input and output accesses of the stage. Nevertheless, its operation philosophy differs from that inherent to other branch-line hybrid-based dual-band BPFs previously reported, where the coupler was tuned within the dual-passband range to contribute to the filtering function under transversal signal-interference techniques [39]. Note also that, in the current circuit, an additional variable capacitor has been inserted in one of the low-impedance arms of the couplers. As attested to here, this was done to further increase its reconfiguration capability in terms of bandwidth control for the dual passbands so that comparable bandwidths for both of them can be achieved. It must be further noticed that, in this particular implementation of the engineered reconfigurable multi-band BPF concept aimed at attaining wideband characteristics, the transmission-line segments of the detuned branch-line couplers also affect the absolute positioning of the dual transmission bands.

The simulated (assuming ideal variable capacitors) and measured power transmission and reflection parameters of the manufactured prototype have been compared for several reconfiguration states [they are set by acting on the adjustable capacitors of the resonators ($C_{r1}$ and $C_{r2}$) and the branch-line couplers ($C_c$)], as next described. Since $C_{r1}$ and $C_{r2}$ are attached to the longest and shortest resonators, respectively, they mostly control the frequency tuning process of the lower

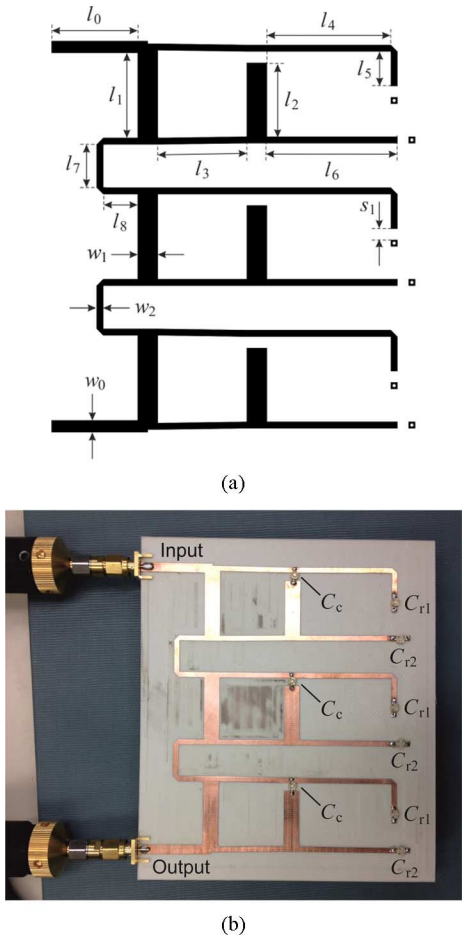


Fig. 9. Layout and photograph of the manufactured reconfigurable wideband dual-band BPF microstrip prototype. (a) Layout ($l_0 = 25.4$ mm, $l_1 = 25$ mm, $l_2 = 21.7$ mm, $l_3 = 26.3$ mm, $l_4 = 36.6$ mm, $l_5 = 10.2$ mm, $l_6 = 38.5$ mm, $l_7 = 12.7$ mm, $l_8 = 10.2$ mm, $w_0 = 3.5$ mm, $w_1 = 5.9$ mm, $w_2 = 1.9$ mm, and $s_1 = 3.3$ mm). (b) Photograph.

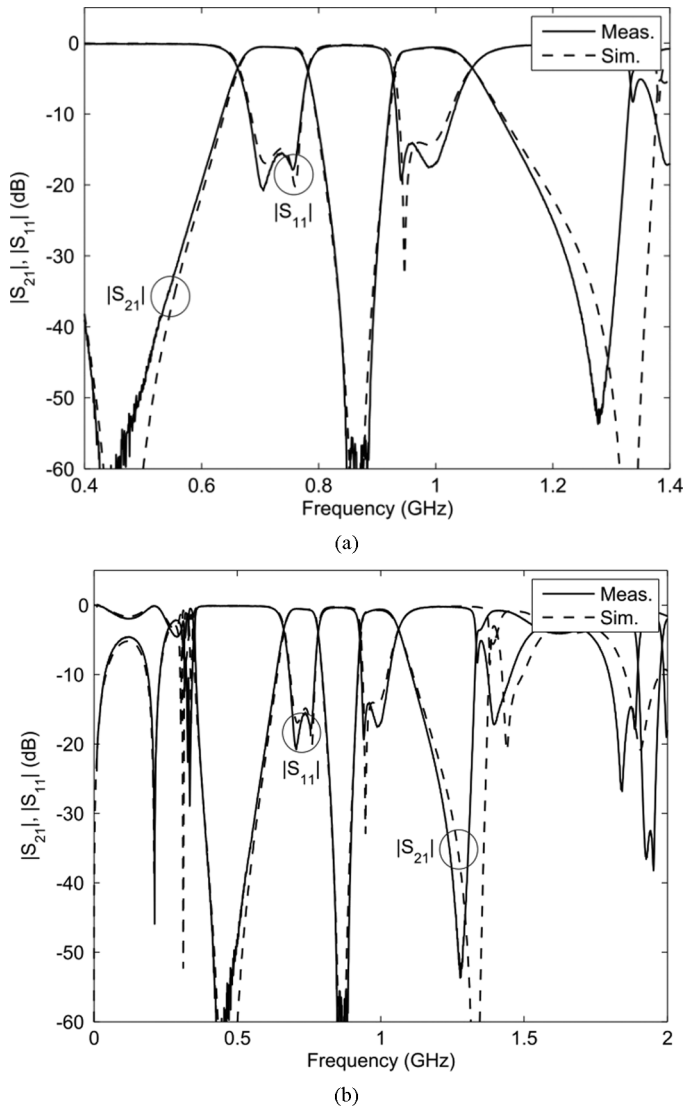


Fig. 10. Simulated and measured power transmission ($|S_{21}|$) and reflection ($|S_{11}|$) responses of the reconfigurable wideband dual-band bandpass microstrip filter prototype: example of equal absolute bandwidths for passbands ($C_{r1} = 2.7$ pF, $C_{r2} = 0.6$ pF, and $C_c = 5.2$ pF). (a) In-band detail. (b) Broadband response.

and upper passbands of the built prototype, respectively. In particular, the center frequencies of the lower and upper passbands are decreased (increased) when higher (lower) values for $C_{r1}$ and $C_{r2}$, respectively, are set (since the resonance frequency $f_{\text{res}}$ of each isolated tunable resonator connected to the detuned branch-line coupler follows the well-known implicit law $f_{\text{res}} = 1/(2\pi C_r Z_r \tan\theta_r(f_{\text{res}}))$ where $C_r$, $Z_r$, and $\theta_r(f_{\text{res}})$ are the capacitance, characteristic impedance, and electrical length at $f_{\text{res}}$ of the capacitor and transmission-line segment of the tunable resonator, respectively). Nevertheless, even in situations where only one passband is reconfigured, the capacitor of the opposite resonators and that of the detuned couplers can need to be readjusted to maintain in-band power matching levels and bandwidths at the two passbands. This is because both resonators interact through the lines of the same detuned branch-line coupler so that the tuning process of one of them slightly alters the effective couplings existing between the resonators that shape the other transmission band.

Fig. 10 shows an example of a dual-band response with nearly equal absolute bandwidths for the passbands (in-band detail and wideband response). The measured characteristics for the lower and upper transmission bands, respectively, are: center frequencies of 0.72 and 1 GHz, 3-dB passband widths equal to 120 and 130 MHz (i.e., of 16.7% and 13% in relative terms), minimum in-band power insertion losses of 0.55 and 0.6 dB, and in-band power matching levels greater than 15.5 and 14.1 dB. Note also from Fig. 10(b), as explained in Section II [see Fig. 3(b)], that the dual-band bandpass filtering action is generated within a wide-stopband range inherent to the quasi-BPF scheme. If necessary in the addressed application, this bandstop spectral interval can be further enlarged through different well-known techniques. Some of these procedures, whose effectiveness has been extensively verified in the past, are as follows: 1) the utilization of interdigital-type coupled-line input/output feeding stages in the whole filter (see, e.g., [40] and [41]) or 2) its simple cascade with an external broadband BPF (e.g., multi-mode type, optimum short-circuited stub approach, or composite high-/low-pass section solution [42], [43]). In the latter, the passband of the wideband BPF must cover the spectral bandwidth within which

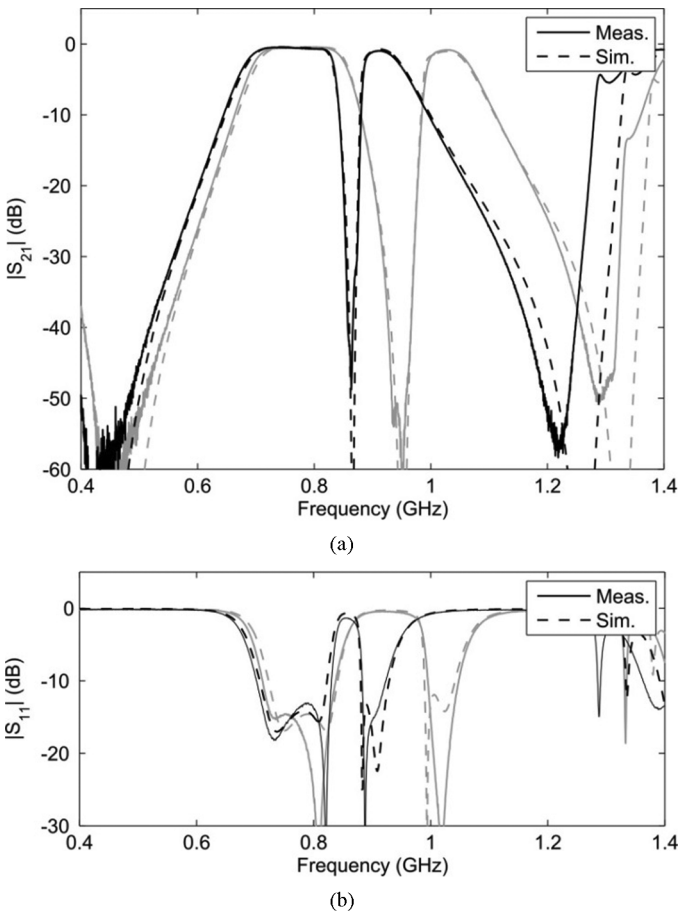


Fig. 11. Simulated and measured power transmission ($|S_{21}|$) and reflection ($|S_{11}|$) responses of the reconfigurable wideband dual-band BPF microstrip prototype: example of center-frequency tuning of the upper passband (black color: $C_{r1} = 3.2$ pF, $C_{r2} = 1.5$ pF, and $C_c = 2.4$ pF; grey color: $C_{r1} = 2.9$ pF, $C_{r2} = 0.6$ pF, and $C_c = 2.5$ pF). (a) $|S_{21}|$. (b) $|S_{11}|$.

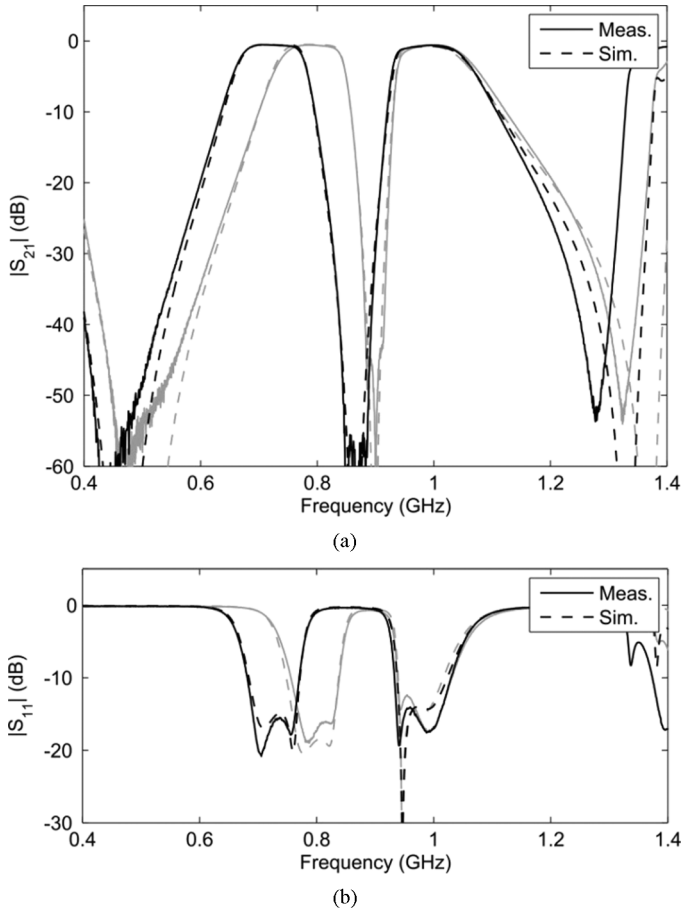


Fig. 12. Simulated and measured power transmission ($|S_{21}|$) and reflection ($|S_{11}|$) responses of the reconfigurable wideband dual-band BPF microstrip prototype: example of center-frequency tuning of the lower passband (black color: $C_{r1} = 2.7$ pF, $C_{r2} = 0.6$ pF, and $C_c = 5.2$ pF; grey color: $C_{r1} = 1.7$ pF, $C_{r2} = 0.6$ pF, and $C_c = 4.5$ pF). (a) $|S_{21}|$. (b) $|S_{11}|$.

the multi-band BPF is reconfigured, but being obviously narrower than that of the broad stopband inherent to its quasi-bandpass topology.

The center-frequency tuning ability of the prototype is illustrated in Figs. 11 and 12. Specifically, Fig. 11 shows how the upper passband is tuned from 0.9 to 1.05 GHz, while the lower one approximately stays fixed at 0.77 GHz. Between these frequencies, the 3-dB absolute bandwidth and minimum in-band insertion loss of the upper passband vary in the ranges of 70–80 MHz and 0.85–1 dB, respectively. In both cases, the in-band power matching levels are higher than 13 dB.

Analogous results are demonstrated in Fig. 12 regarding the center-frequency agility of the lower passband. In particular, this band is tuned from 0.72 to 0.8 GHz, while the upper one is maintained fixed at 1 GHz. The 3-dB bandwidth and minimum in-band transmission loss for the lower passband are 120 MHz and 0.55 dB in both filtering profiles, respectively, and the in-band power matching levels are greater than 15.5 dB.

In relation with the center-frequency tuning capability of this prototype (and apart from the obvious limitations imposed by the wideband stopband inherent to the quasi-bandpass scheme, which shows a relative bandwidth of about 115% in this case, and the variation ranges of the adjustable capacitors), it should be noticed that the maximum spectral separation feasible between passbands comes constrained by the deterioration of the in-band power matching levels as the inter-passband spacing is increased. For this particular circuit and depending on bandwidth states, a relative upper to lower center-frequency separation from 1.7 to 1.8 can be achieved for minimum in-band power matching levels of 10 dB.

Fig. 13 exemplifies the bandwidth-control feature for the dual passbands. Here, two different tuned dual-band bandpass transfer functions are depicted, as follows: the first one with a wideband lower passband (160-MHz 3-dB bandwidth around 0.78 GHz, i.e., of 20.5%) and a moderate-bandwidth upper passband (3-dB bandwidth of 70 MHz centered at 0.97 GHz, i.e., of 7.2%), whereas the second one shows a moderate-bandwidth lower passband (70-MHz 3-dB bandwidth around 0.69 GHz, i.e., of 10.1%) and a broadband upper passband (3-dB bandwidth of 150 MHz centered at 0.85 GHz, i.e., of 17.6%). For these filtering actions, comparable performances in terms of in-band power insertion loss and matching levels to those of the previous responses are obtained. Further bandwidth flexibility is feasible either by using different $C_c$ capacitors in the detuned branch-line coupler of each stage or through alternative realizations of the devised reconfigurable multi-band BPF concept as attested by the second prototype.

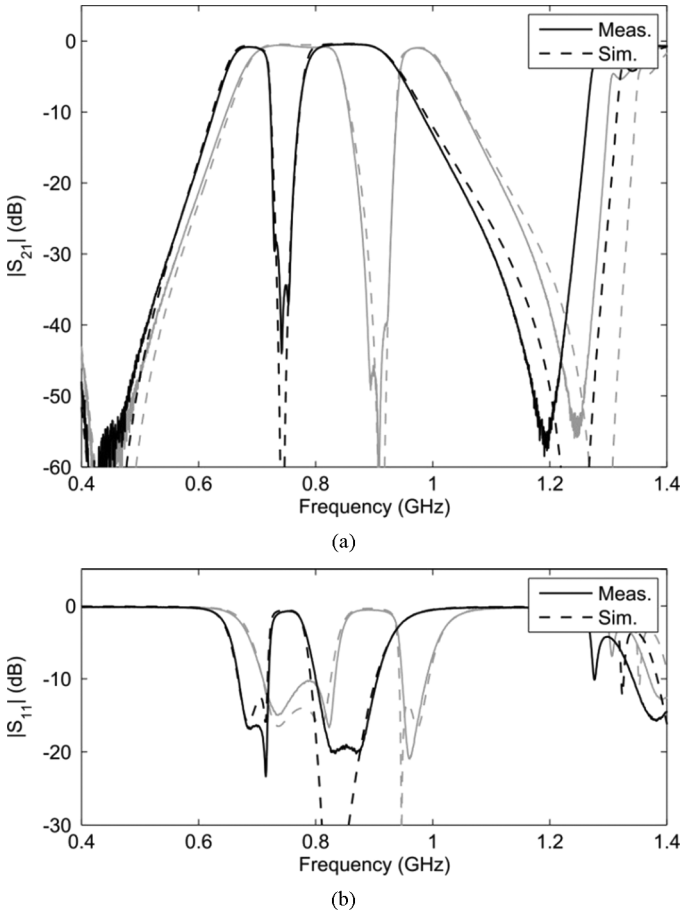


Fig. 13. Simulated and measured power transmission ($|S_{21}|$) and reflection ($|S_{11}|$) responses of the reconfigurable wideband dual-band BPF microstrip prototype: example of bandwidth tuning (black color: $C_{r1} = 3$ pF, $C_{r2} = 1.8$ pF, and $C_c = 5.4$ pF; grey color: $C_{r1} = 3.2$ pF, $C_{r2} = 1$ pF, and $C_c = 2.5$ pF). (a) $|S_{21}|$. (b) $|S_{11}|$.

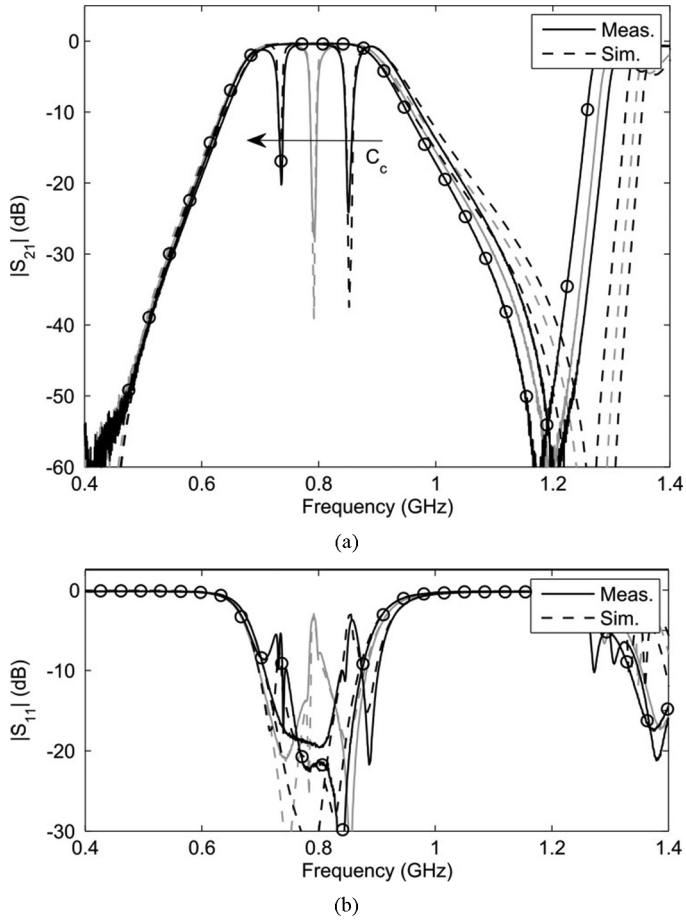


Fig. 14. Simulated and measured power transmission ($|S_{21}|$) and reflection ($|S_{11}|$) responses of the reconfigurable wideband dual-band BPF microstrip prototype: example of broadband single-band BPF response with in-band tunable notch (black color: $C_{r1} = 2.8$ pF, $C_{r2} = 2.9$ pF, and $C_c = 1.5$ pF; grey color: $C_{r1} = 2.7$ pF, $C_{r2} = 3.4$ pF, and $C_c = 2.1$ pF; black color with circle: $C_{r1} = 2.8$ pF, $C_{r2} = 2.9$ pF, and $C_c = 3.7$ pF). (a) $|S_{21}|$. (b) $|S_{11}|$.

Finally, additional operation states feasible through the built reconfigurable wideband dual-band BPF circuit are shown. Specifically, Fig. 14 verifies how this prototype can also work as broadband BPF with an in-band frequency-tunable notch when the two passbands are almost merged together. Moreover, as can be seen, the spectral control of the notch is carried out by mainly acting on the capacitors of the branch-line hybrids, while nearly maintaining the performance of the entire transfer function. Indeed, an overall passband with an absolute 3-dB bandwidth of about 270 MHz around 0.8 GHz (i.e., equal to 34% in relative terms) and minimum in-band transmission loss of 0.3 dB is measured for the three responses. This reveals another feature of this reconfigurable multi-band BPF scheme that is further verified in the second prototype: the synthesis of wider band BPFs through multi-passband aggregation, therefore overcoming maximum-bandwidth limits of classic coupled-line BPFs with single-mode resonators due to technological restrictions imposed by minimum realizable coupled-line physical separations.

### *B. Prototype 2: Narrowband Quadruple-Band BPF*

The second circuit is a quad-band BPF with fully adaptive narrowband passbands within the frequency interval of 0.8–1.4 GHz. For its design, a pair of two-stage versions of the general quasi-BPF scheme shown in Fig. 2(a), each one having a couple of mono-frequency resonators interacting with the NRNs, were arranged in a parallel-type two-path transversal network. Thus, its coupling-node topology exactly corresponds to the one provided in Fig. 4 (the 180° phase delay between the two paths was realized in this prototype with an additional transmission-line segment in one of them). Such flexible structure permits optimum performance to be obtained for all the filtering states, which encompasses the generation of inter-band TZs for high selectivity in multi-band filtering states or the dynamic merging of several passbands to conform broader and even higher order transmission bands.

The layout and a photograph of the manufactured prototype are shown in Fig. 15. Nonredundant physical dimensions are also provided. As in the previous example, the resonators have been implemented as a transmission-line segment ended in a short-circuited variable lumped capacitor at its edge. Nevertheless, in contrast to the dual-band circuit of Fig. 9, all the resonating lines have the same physical length in this case. Therefore, as indicated in Fig. 15(a) and accordingly to the operating principle of this reconfigurable multi-band BPF approach, four different values for the capacitors of the resonators ($C_{r1}$, $C_{r2}$, $C_{r3}$, and $C_{r4}$) should be considered in the tuning

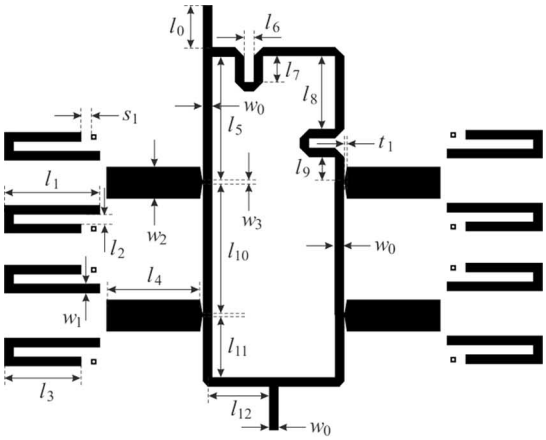


(a)

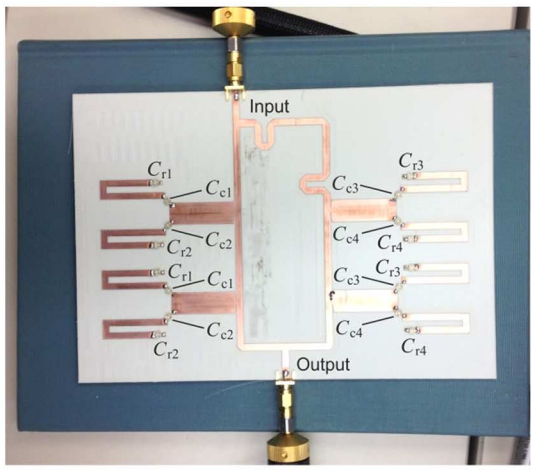


(b)

Fig. 15. Layout and photograph of the manufactured reconfigurable narrowband quad-band BPF microstrip prototype. (a) Layout ($l_0 = 16.6$ mm, $l_1 = 33.8$ mm, $l_2 = 3.3$ mm, $l_3 = 27.2$ mm, $l_4 = 33$ mm, $l_5 = 45.8$ mm, $l_6 = 3.3$ mm, $l_7 = 9.1$ mm, $l_8 = 25.6$ mm, $l_9 = 8.8$ mm, $l_{10} = 46.5$ mm, $l_{11} = 22$ mm, $l_{12} = 21.7$ mm, $w_0 = 3.3$ mm, $w_1 = 3.3$ mm, $w_2 = 11.2$ mm, $w_3 = 1.5$ mm, $s_1 = 3.4$ mm, and $t_1 = 0.9$ mm). (b) Photograph.

process of quadruple-band filtering transfer functions with two-pole passbands. Note also that the interactions between the NRNs of each quasi-bandpass section have been realized here by means of low-impedance/capacitive-type transmission-line sections, which connect the transversal paths and the resonators through variable capacitors ($C_{c1}$, $C_{c2}$, $C_{c3}$, and $C_{c4}$). This was done to generate the required effectively adjustable weak signal couplings between the filter resonators towards the achievement of ultra-high levels of reconfiguration.

A demonstration of a configured quad-band bandpass filtering response (simulated and measured power transmission and reflection parameters) with nearly equal absolute bandwidths for the passbands isolated by inter-band TZs is illustrated in Fig. 16. As can be seen, four second-order passbands are attained, where the homologous resonators of the transversal branches contribute as poles for the same transmission band. In this particular response, the resonators with $C_{r1}$, $C_{r4}$, $C_{r3}$, and $C_{r2}$ capacitors, respectively, shape the first, second, third, and fourth transmission bands (since $C_{r1} > C_{r4} > C_{r3} > C_{r2}$ in this case). Thus, the center frequencies of these passbands can be varied by acting on the aforementioned capacitors, as

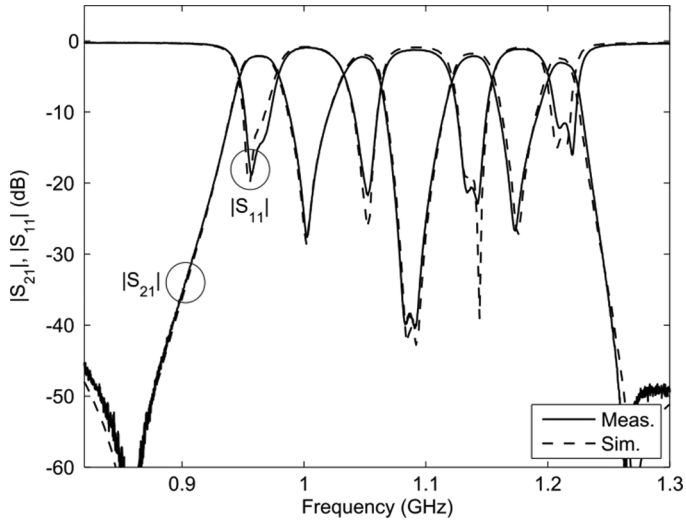


Fig. 16. Simulated and measured power transmission ($|S_{21}|$) and reflection ($|S_{11}|$) responses of the reconfigurable narrowband quad-band BPF microstrip prototype: example of quadruple-passband filtering state ($C_{r1} = 3.2$ pF, $C_{r2} = 1$ pF, $C_{r3} = 1.4$ pF, $C_{r4} = 2$ pF, $C_{c1} = 1.7$ pF, $C_{c2} = 0.9$ pF, $C_{c3} = 1.3$ pF, and $C_{c4} = 1.6$ pF).

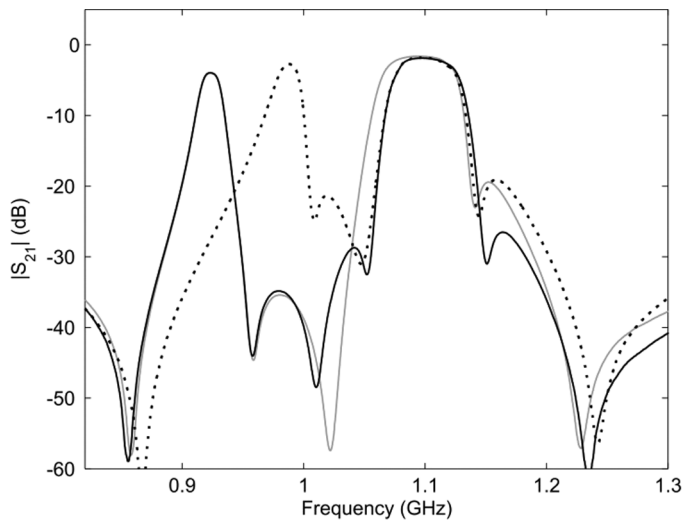


(a)

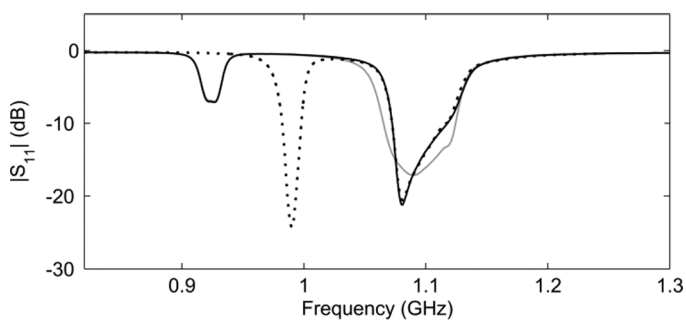


(b)

Fig. 17. Measured power transmission ($|S_{21}|$) and reflection ($|S_{11}|$) responses of the reconfigurable narrowband quad-band BPF microstrip prototype: examples of dual-passband filtering states. (a) $|S_{21}|$. (b) $|S_{11}|$.

explained in Section III-A for the first prototype. Furthermore, a nearly independent bandwidth reconfiguration for each passband is feasible in this prototype almost without affecting the other three transmission bands by only adjusting the $C_r$ and $C_c$ capacitors associated to the passband to be tuned (that

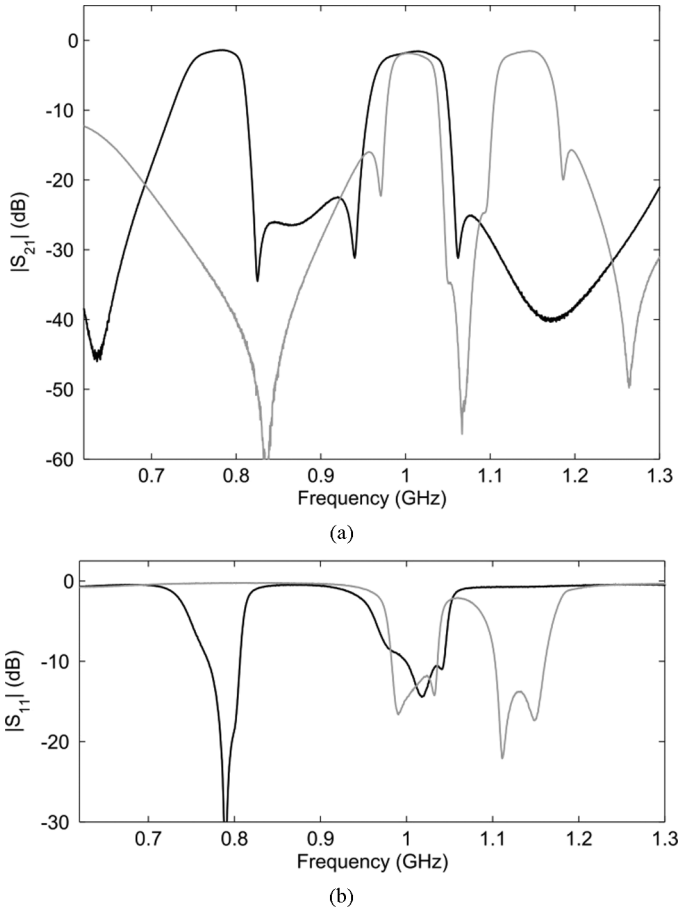


Fig. 18. Measured power transmission ($|S_{21}|$) and reflection ($|S_{11}|$) responses of the reconfigurable narrowband quad-band BPF microstrip prototype: example of simultaneous dual-passband frequency tuning throughout a broad spectral range. (a) $|S_{21}|$. (b) $|S_{11}|$.

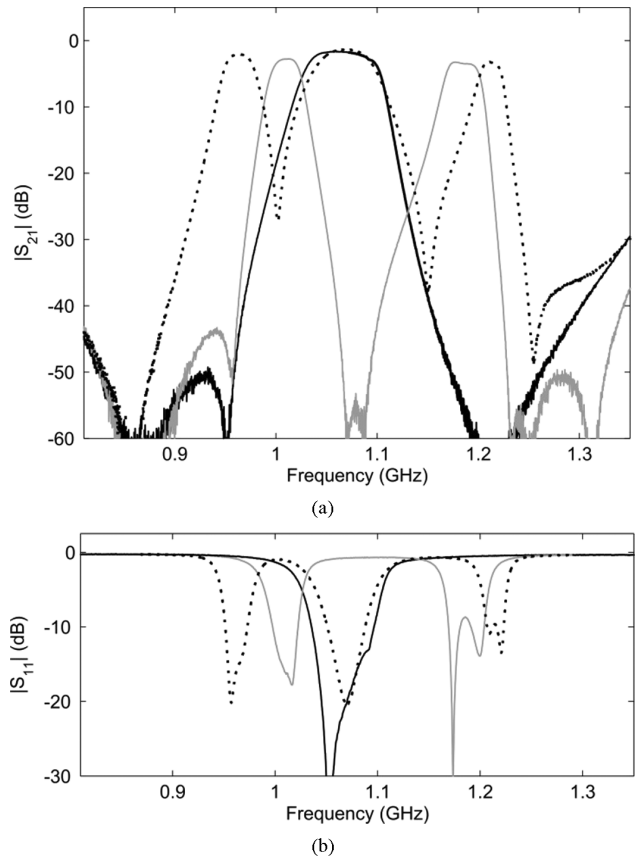


Fig. 19. Measured power transmission ($|S_{21}|$) and reflection ($|S_{11}|$) responses of the reconfigurable narrowband quad-band BPF microstrip prototype: examples of single-, dual-, and triple-passband filtering states. (a) $|S_{21}|$. (b) $|S_{11}|$.

theoretically for very low values of $C_c$ (i.e., as the bandwidth is decreased) would result in the limit in that passband to be intrinsically switched off). The measured performances for its transmission bands, listed from the lower to the upper one, are: center frequencies equal to 0.96, 1.05, 1.14, and 1.21 GHz, 3-dB absolute passband widths of 33, 31, 31, and 26 MHz (i.e., of 3.4%, 3%, 2.7%, and 2.2% in relative terms), and minimum in-band power insertion losses of 2.1, 2.2, 2.1, and 3 dB. In-band power matching levels greater than 11.6 dB are obtained for all the passbands.

In the following, some representative examples confirming the reconfiguration capability of the built prototype are shown. Note also that for the sake of clarity, although the same fairly close agreement between experimental and predicted results as in the previous tuned responses can be verified for all the configured states, only measured results are reported hereafter. Moreover, due to the very-high reconfiguration capability of this multi-band BPF device, it is not always possible to derive simple reconfiguration laws for setting one specific filtering function starting from another one (e.g., from a quad-band response to a single-band filtering action with linear phase profile, due to the very different coupling matrices associated to both filtering functions). This is also the case of some other previous approaches reported in the technical literature, which involve coupling manipulation for tuning, despite being mainly restricted to reconfigurable single-band BPFs (e.g., the field-programmable filter array (FPFA) of [16]). Especially for an electronically reconfigurable version of this filter, this could be circumvented in practice by means of an auxiliary digital subsystem enabling its automatic tuning from the previously extracted and stored filter states of interest.

Fig. 17 depicts the measured power transmission and reflection responses of the circuit for three different dual-band bandpass filtering states, where a quasi-elliptic-type higher order upper passband has been synthesized by congregating multiple poles in the same transmission range. As can be seen, an independent control for each passband is feasible. Specifically, it is shown how a nearly constant-absolute-bandwidth frequency tuning for a 20-MHz 3-dB-bandwidth lower passband is accomplished between 0.92–0.99 GHz, whereas the upper one remains centered at 1.1 GHz. Besides, it is confirmed that the upper passband can be finely adjusted in terms of 3-dB bandwidth (between 55–62 MHz in this example) without exhibiting undesired frequency-deviation effects inherent to other reconfigurable topologies (e.g., see [14]), while nearly keeping fixed the lower passband.

Furthermore, this multi-passband filtering function can be arbitrarily generated throughout the full-tuning bandwidth (it comes mainly determined by the variation ranges of the variable capacitors employed as tuning elements) with very flexible specifications for the passbands and the inter-band frequency

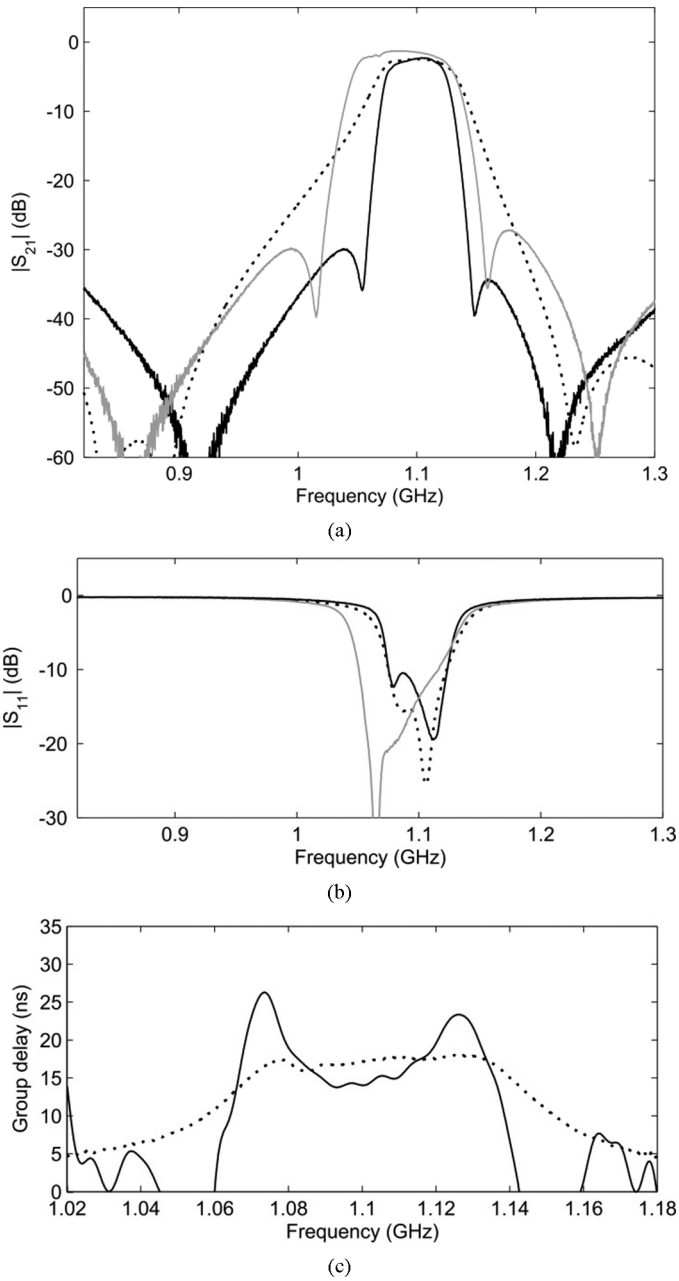


Fig. 20. Measured power transmission ($|S_{21}|$), reflection ($|S_{11}|$) and smoothed group-delay responses of the reconfigurable narrowband quad-band BPF microstrip prototype: examples of single-passband filtering states (including quasi-elliptic-type and self-equalized flat-group-delay transfer functions). (a) $|S_{21}|$. (b) $|S_{11}|$. (c) Smoothed group delay (passband detail).

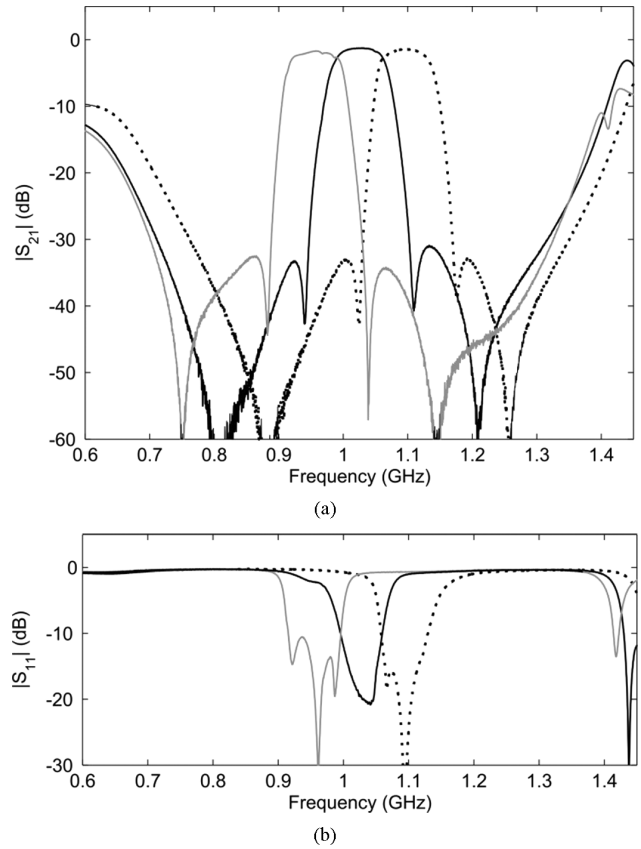


Fig. 21. Measured power transmission ($|S_{21}|$) and reflection ($|S_{11}|$) responses of the reconfigurable narrowband quad-band BPF microstrip prototype: examples of frequency-contiguous quasi-elliptic-type single-passband filtering states with tuned center frequency and constant absolute bandwidth. (a) $|S_{21}|$. (b) $|S_{11}|$.

spacing. Regarding the latter, two additional sharp-rejection dual-passband responses with several TZs are drawn in Fig. 18 for the wideband range of 0.6–1.3 GHz. The first filtering profile, reconfigured in the lower part of the entire tuning range, has its lower and upper passbands located at 0.78 and 1 GHz with 3-dB absolute bandwidths of 60 and 80 MHz (i.e., relative bandwidths of 7.7% and 8%). The second response, tuned in the upper region of the represented spectral interval, shows lower and upper transmission bands with center frequencies of 1 and 1.15 GHz and 3-dB absolute bandwidths of 55 and 69 MHz (equivalently, of 5.5% and 6% in relative terms). For both passbands of these dual-band bandpass filtering transfer functions, minimum in-band power insertion losses of 1.8 dB are attained.

Fig. 19 exemplifies the transformation of a mono-band bandpass filtering transfer function into two multi-passband responses exhibiting two and three transmission bands, respectively. Initially, a moderate-bandwidth quasi-elliptic-type bandpass filtering profile with a 3-dB absolute bandwidth of 80 MHz around 1.06 GHz (i.e., of 7.5% in relative terms), minimum in-band power transmission losses of 1.6 dB, and multiple stopband TZs was set. By reconfiguring the natural frequencies of the filter resonators, it is then proven how their associated poles can be split to create a dual-band bandpass filtering action with narrow-bandwidth passbands (note that, due to the high-$Q$ characteristics of the mechanically adjustable capacitors, passband widths as small as those attainable in related coupled-resonator BPF schemes for such frequency ranges and microstrip substrate can be set). In this case, the passbands are located at 1 and 1.18 GHz, showing 3-dB absolute bandwidths of 32 and 34 MHz (i.e., of about 3% in relative terms for both transmission bands), and in-band power transmission losses higher than 2.8 and 3.2 dB, respectively. Subsequently, such dynamic-pole allocation capability is applied to set a triple-passband filtering function. Now, its lower to upper passbands are centered at 0.96, 1.06, and 1.22 GHz with 3-dB absolute bandwidths equal to 33, 62, and 22 MHz (i.e., relative

TABLE I
COMPARISON OF THE PROPOSED RECONFIGURABLE MULTI-BAND BPF APPROACH WITH THE STATE-OF-THE-ART [22]–[30]

| | [22] | [23] | [24] | [25], [26] | [27] | [28] | [29] | [30] | This work |
|---|---|---|---|---|---|---|---|---|---|
| **Technology** | Microstrip + varactors | Microstrip + varactors | Microstrip + varactors | Microstrip + varactors | Microstrip + varactors | Coaxial cavity + actuators | Microstrip + p-i-n diodes | Microstrip + varactors | Microstrip + trimmer caps. |
| **Approach** | Recursive active BPF | λ/4 resonators + bandstop stubs | Stub-loaded resonators | Dual-mode resonators | λ/4/step-line resonators | Intersected resonators | Controllable DGS | Switchable filter bank | Quasi-bandpass network |
| **Type of tuning** | Continuous | Continuous | Continuous | Continuous | Continuous | Continuous | Discrete | Mixed | Continuous |
| **Number of passbands** | 2 | 2 | 2 | 2 | 2 | 2 | 3 | 3 (valid for *N*) | 1-4 (valid for *N*) |
| **Frequency tuning** | ✓ | ✓ | ✓ | ✓ | ✓ | ✓ | — | ✓ | ✓ |
| **Bandwidth tuning** | — | — | — | ✓ | ✓ | — | — | ✓ | ✓ |
| **TZ generation** | — | ✓ | ✓ | ✓ | ✓ | ✓ | ✓ | ✓ | ✓ |
| **Reconfigurable order** | — | — | — | — | — | — | — | — | ✓ |
| **Band number control** | — | — | — | — | — | — | ✓ | ✓ | ✓ |
| **Additional functionalities** | — | — | — | — | — | — | — | — | ✓ |

*Note*: "Additional functionalities" refer to operation modes as single-band BPF with reconfiguration capability in terms of center frequency, bandwidth, group-delay, TZ, filtering function (e.g., equiripple, maximally flat, and quasi-elliptic linear-phase type) and even with in-band adjustable notches.

bandwidths of 3.5%, 5.9%, and 1.8%). The in-band minimum power transmission loss levels are 2.1, 1.3, and 3.2 dB.

Subsequently, as further reconfiguration flexibility, the capability of the fabricated reconfigurable multi-band BPF prototype to also operate as a linear-phase BPF is demonstrated. Note that flat group-delay BPFs are very desirable for a variety of applications such as digital communications, where phase-distortion requirements can become more stringent than amplitude-distortion characteristics [44].

In relation to the latter, the measured power transmission, reflection, and smoothed group-delay curves for three single-passband filtering states of the constructed circuit are plotted in Fig. 20. Two of them, which correspond to quasi-elliptic-type transfer functions, validate how the bandwidth and the TZs can be simultaneously tuned to maintain the selectivity performance. In particular, for these curves, the 3-dB bandwidth is varied from 50 to 80 MHz (i.e., from 4.5% to 7.5% in relative terms) while preserving the out-of-band rejection levels and sharpness of the cutoff slopes. On the contrary, the effective coupling values giving rise to the creation of the adjacent-to-passband real TZs in the aforementioned transfer functions have been reconfigured in the third response for self-equalization purpose at the expense of selectivity reduction. This is confirmed in Fig. 20(c), which attests to a reduction in the maximum in-band group-delay variation from 17 ns (quasi-elliptic-type narrower-band response) to 2.2 ns (self-equalized response) for a nearly similar transmission range.

To conclude, the center-frequency tuning ability of the constructed reconfigurable multi-band BPF prototype when acting as single-band BPF is confirmed in Fig. 21. In this figure, the measured power transmission and reflection responses of three contiguous-frequency quasi-elliptic-type BPF states with equal absolute bandwidths are represented. As explained in Section II [see Fig. 3(b)] and also shown in Fig. 10(b) for the first prototype, it is observed that the bandpass filtering function is generated within a broad stopband range inherent to the quasi-bandpass stages embodied in the overall BPF transversal branches. The main performances for the measured passbands, enumerated from the lower to the upper spectrally tuned transfer function, are as follows: center frequencies of 0.96, 1.03, and 1.1 GHz, 3-dB absolute bandwidths equal to 85, 85, and 84 MHz (i.e., of 8.9%, 8.3%, and 7.6% in relative terms), minimum in-band power transmission loss of 1.7, 1.3, and 1.4 dB, and in-band power matching levels higher than 10 dB in all the responses. Note that, in contrast to other available techniques to design constant absolute-bandwidth tunable-center frequency BPFs, such a feature is achieved here through the dynamic-pole allocation instead of by complicated methods to attain the required variation patterns versus tuned center frequency for the inter-resonator couplings (e.g., dual-mode resonators and stepped-impedance/corrugated lines properly arranged) within the entire tuning range [45]–[49]. Moreover, adjacent TZs are created at both passband sides in all the tuned states, as a benefit in relation to most of related past solutions.

### C. Comparison With State-of-the-Art

A qualitative comparative study of the main features of the proposed reconfigurable multi-band BPF approach in relation to those of the state-of-the-art [22]–[30] is given in Table I. In relation to this table, the following two clarifications should be made.

- Control of the number of passbands (which gives rise to an equivalent "passband-switching" effect) and order re-

configuration refer, respectively, to the possibility of dynamically modify the amount of generated transmission bands and their building poles in the same circuit. As was previously shown, this can be accomplished in the current multi-band BPF by two different ways: 1) through the passband-merging feature when all the tunable resonators are utilized to configure transmission bands or 2) by detuning a subset of reconfigurable resonators that remain unused for passband shaping.

- Additional functionalities mean the potential of setting reconfiguration states other than the multi-passband one. In this case, they are tune-all broadband bandpass filtering with in-band adjustable notches or self-equalized quasi-elliptic-type bandpass filtering with linear-phase performance.

## IV. Conclusion

A new family of frequency-agile multi-band microwave BFPs with fully reconfigurable transmission bands has been proposed. It is based on a quasi-BPF configuration with multi-band operation, which comprises distinct sets of controllable mono-frequency resonators to separately generate each tunable passband. It enables unprecedented levels of reconfiguration to be attained in the same circuit, which acts as multi-mode/multi-purpose filtering device. Examples encompass high-selectivity multi-band states with center-frequency- and bandwidth-adaptive passbands or wider band/higher order single-band bandpass responses through passband merging, which exhibit tune-all capability in terms of center frequency, bandwidth, TZs, group delay, and in-band notches. Furthermore, the reported multi-band BPF approach is generalizable to synthesize any number of passbands and is well suited for different tunable resonator and filter technologies. The theoretical principles of the devised reconfigurable multi-band BFP structure, with an emphasis on the analysis of the quasi-bandpass section as a basic building block, have been described through the coupling-node formalism along with a triple-band BPF synthesis example. In addition, to experimentally validate the concept, two different fully adaptive multi-band BPF prototypes incorporating mechanically variable capacitors for high-$Q$ tuning have been successfully developed in microstrip substrate and measured.

They were a three-pole broadband dual-band BPF and a narrowband quadruple-passband filter with a merging feature for its transmission bands by using a two-path transversal configuration. To the authors' knowledge, the engineered frequency-adaptive multi-band BFP approach has demonstrated the highest reconfiguration capability reported to date for this class of devices. Future research work to be addressed is the realization of an electronically controllable version of these reconfigurable multi-band BPFs by using varactor diodes as variable reactance elements, along with its complete characterization in terms of power-handling/linearity behavior. The development of an auxiliary digital subsystem for its automatic electronic reconfiguration remains also as further work to be carried out.

## Acknowledgment

Author R. Gómez-García would like to express his gratitude to the Defense Advanced Research Project Agency (DARPA), Project Manager Dr. W. J. Chappell and to the Office of Naval Research Global (ONRG) for their support.

The views expressed are those of the authors and do not reflect the official policy or position of the Department of Defense or the U.S. Government. Distribution Statement "A" (Approved for Public Release, Distribution Unlimited).

## References

[1] J.-S. Hong, "Reconfigurable planar filters," *IEEE Microw. Mag.*, vol. 10, no. 6, pp. 73–83, Oct. 2009.

[2] J. Sun, C. Li, Y. Geng, and P. Wang, "A highly-reconfigurable low-power CMOS directional coupler," *IEEE Trans. Microw. Theory Techn.*, vol. 60, no. 9, pp. 2815–2822, Sep. 2012.

[3] D. Patron, D. Piazza, and K. R. Dandekar, "Wide-band planar antenna with reconfigurable omnidirectional and directional radiation patters," *IET Electron. Lett.*, vol. 49, no. 8, pp. 516–518, Apr. 2013.

[4] J. J. Kim, K.-H. Lee, J. Choi, Y. Park, K. Lim, and C.-H. Lee, "Ultra-wideband CMOS voltage-controlled oscillator with reconfigurable tunable inductors," *IET Electron. Lett.*, vol. 47, no. 4, pp. 249–250, Feb. 2011.

[5] U. Kim, S. Kang, J. Woo, Y. Kwon, and J. Kim, "A multi-band reconfigurable power amplifier for UMTS handset applications," *IEEE Trans. Microw. Theory Techn.*, vol. 60, no. 8, pp. 2532–2542, Aug. 2012.

[6] P. Cruz, N. B. Carvalho, and K. A. Remley, "Designing and testing software-defined radios," *IEEE Microw. Mag.*, vol. 11, no. 4, pp. 83–94, Jun. 2010.

[7] P. W. East, "Fifty years of instantaneous frequency measurement," *IET Radar, Sonar Navigat.*, vol. 6, no. 1, pp. 112–122, Mar. 2012.

[8] I. C. Hunter and J. D. Rhodes, "Electronically tunable microwave bandpass filters," *IEEE Trans. Microw. Theory Techn.*, vol. MTT-30, no. 9, pp. 1354–1360, Sep. 1982.

[9] S. Courrèges, Y. Li, Z. Zhao, K. Choi, A. Hunt, and J. Papapolymerou, "A low-loss X-band quasi-elliptic ferroelectric tunable filter," *IEEE Microw. Wireless Compon. Lett.*, vol. 19, no. 4, pp. 203–205, Apr. 2009.

[10] G. Rebeiz, K. Entesari, I. Reines, S.-J. Park, M. El-tanani, A. Grichener, and A. Brown, "Tuning in to RF MEMS," *IEEE Microw. Mag.*, vol. 10, no. 6, pp. 55–72, Oct. 2009.

[11] X. Liu, L. P. B. Katehi, W. J. Chappell, and D. Peroulis, "High-$Q$ tunable microwave cavity resonators and filters using SOI-based RF MEMS tuners," *J. Microelectromech. Syst.*, vol. 4, no. 4, pp. 230–237, Dec. 1995.

[12] T.-Y. Yun and K. Chang, "Piezoelectric-transducer-controlled tunable microwave circuits," *IEEE Trans. Microw. Theory Techn.*, vol. 50, no. 5, pp. 1303–1310, May 2002.

[13] M. Yazdanpanahi and D. Mirshekar-Syahkal, "Millimeter-wave liquid-crystal-based tunable bandpass filter," in *IEEE Radio Wireless Symp.*, New Orleans, LO, USA, Jan. 10–14, 2010, pp. 139–142.

[14] M. Sánchez-Renedo, R. Gómez-García, J. I. Alonso, and C. Briso-Rodríguez, "Tunable combline filter with continuous control of center frequency and bandwidth," *IEEE Trans. Microw. Theory Techn.*, vol. 53, no. 1, pp. 191–199, Jan. 2005.

[15] A. C. Guyette, "Alternative architectures for narrowband varactor-tuned bandpass filters," in *39th Eur. Microw. Conf.*, Rome, Italy, Sep. 28– Oct. 2, 2009, pp. 1828–1831.

[16] J. Lee, E. J. Naglich, H. H. Sigmarsson, D. Peroulis, and W. J. Chappell, "Tunable inter-resonator coupling structure with positive and negative values and its application to the field-programmable filter array (FPFA)," *IEEE Trans. Microw. Theory Techn.*, vol. 59, no. 12, pp. 3389–3400, Dec. 2011.

[17] B. Yassini, M. Yu, and B. Keats, "A $Ka$-band fully tunable cavity filter," *IEEE Trans. Microw. Theory Techn.*, vol. 60, no. 12, pp. 4002–4012, Dec. 2012.

[18] J.-R. Mao, W.-W. Choi, K.-W. Tam, W. Q. Che, and Q. Xue, "Tunable bandpass filter design based on external quality factor tuning and multiple mode resonators for wideband applications," *IEEE Trans. Microw. Theory Techn.*, vol. 61, no. 7, pp. 2574–2584, Jul. 2013.

[19] M.-A. Sánchez-Soriano, R. Gómez-García, G. Torregrosa-Penalva, and E. Bronchalo, "Bandpass filter with switchable bandwidths between 10–50%," *IET Microw. Antennas Propag.*, vol. 7, no. 7, pp. 502–509, May 2013.

[20] A. C. Guyette, "Theory and design of intrinsically switched multiplexers with optimum phase linearity," *IEEE Trans. Microw. Theory Techn.*, vol. 61, no. 9, pp. 3254–3264, Sep. 2013.

[21] E. J. Naglich, J. Lee, D. Peroulis, and W. J. Chappell, "A tunable bandpass-to-bandstop reconfigurable filter with independent bandwidth and tunable response shape," *IEEE Trans. Microw. Theory Techn.*, vol. 58, no. 12, pp. 3770–3779, Dec. 2010.

[22] D. Segovia-Vargas, O. G. Pérez, V. González-Posadas, and F. Aznar-Ballesta, "Dual-band tunable recursive active filters," *IEEE Microw. Wireless Compon. Lett.*, vol. 21, no. 2, pp. 92–94, Feb. 2011.

[23] E. E. Djoumessi and K. Wu, "Varactor-tuned quarter-wavelength dual-bandpass filter," *IET Microw. Antennas Propag.*, vol. 3, no. 1, pp. 502–509, Jan. 2009.

[24] L. Gao, X. Y. Zhang, B.-J. Hu, and Q. Xue, "Novel multi-stub loaded resonators and their applications to various bandpass filters," *IEEE Trans. Microw. Theory Techn.*, vol. 62, no. 5, pp. 1162–1172, May 2014.

[25] G. Chaudhary, Y. Jeong, and J. Lim, "Dual-band bandpass filter with independently tunable center frequencies and bandwidths," *IEEE Trans. Microw. Theory Techn.*, vol. 61, no. 1, pp. 107–116, Jan. 2013.

[26] X. Huang, L. Zhu, Q. Feng, Q. Xia, and D. Jia, "Tunable bandpass filter with independently controllable dual passbands," *IEEE Trans. Microw. Theory Techn.*, vol. 61, no. 9, pp. 3200–3208, Sep. 2013.

[27] Y. Tao and G. Rebeiz, "Three-pole 1.3–2.4 GHz diplexer and 1.1–2.45 GHz dual-band filter with common resonator topology and flexible tuning capabilities," *IEEE Trans. Microw. Theory Techn.*, vol. 61, no. 10, pp. 3613–3624, Oct. 2013.

[28] E. J. Naglich, J. Lee, H. H. Sigmarsson, D. Peroulis, and W. J. Chappell, "Intersecting parallel-plate waveguide loaded cavities for dual-mode and dual-band filters," *IEEE Trans. Microw. Theory Techn.*, vol. 61, no. 5, pp. 1829–1838, Mar. 2013.

[29] C. K. Chio, S. W. Ting, and K. W. Tang, "Novel reconfigurable multiple-band quasi-elliptic bandpass filter using defected ground structure," in *IEEE MTT-S Int. Microw. Symp.*, Seattle, WA, USA, Jun. 2–7, 2013.

[30] A. C. Guyette, "Intrinsically switched varactor-tuned filters and filter banks," *IEEE Trans. Microw. Theory Techn.*, vol. 60, no. 4, pp. 1044–1056, Apr. 2012.

[31] A. C. Guyette, "Design of fixed- and varactor-tuned bandstop filters with spurious suppression," in *40th Eur. Microw. Conf.*, Paris, France, Sep. 26– Oct. 1, 2010, pp. 292–295.

[32] C.-C. Cheng and G. M. Rebeiz, "A three-pole 1.2–2.6-GHz RF MEMS tunable notch filter with 40-dB rejection and bandwidth control," *IEEE Trans. Microw. Theory Techn.*, vol. 60, no. 8, pp. 2431–2438, Aug. 2012.

[33] Y.-H. Chun, H. Shaman, and J.-S. Hong, "Switchable embedded notch structure for UWB bandpass filter design," *IEEE Microw. Wireless Compon. Lett.*, vol. 18, no. 9, pp. 590–592, Sep. 2008.

[34] Z. Wu, Y. Shim, and M. Rais-Zadeh, "Miniaturized UWB filters integrated with tunable notch filters using a silicon-based integrated passive device technology," *IEEE Trans. Microw. Theory Techn.*, vol. 60, no. 3, pp. 518–527, Mar. 2012.

[35] M. Nosrati, N. Vahabisani, and M. Daneshmand, "A novel ultra wideband (UWB) filter with double tunable notch-bands using MEMS capacitors," in *IEEE MTT-S Int. Microw. Symp.*, Seattle, WA, USA, Jun. 2–7, 2013.

[36] I. C. Hunter, *Theory and Design of Microwave Filters*. London, U.K.: IEE Press, 2001.

[37] R. J. Cameron, "Advanced coupling matrix synthesis techniques for microwave filters," *IEEE Trans. Microw. Theory Techn.*, vol. 51, no. 1, pp. 1–10, Jan. 2003.

[38] J.-S. Hong, *Microstrip Filters for RF/Microwave Applications*, 2nd ed. New York, NY, USA: Wiley, 2011.

[39] R. Gómez-García and M. Sánchez-Renedo, "Microwave dual-band bandpass planar filters based on generalized branch-line couplers," *IEEE Trans. Microw. Theory Techn.*, vol. 58, no. 12, pp. 3760–3769, Dec. 2010.

[40] S. Sun, L. Zhu, and H. H. Tan, "A compact wideband bandpass filter using transversal resonator and asymmetrical interdigital coupled lines," *IEEE Microw. Wireless Compon. Lett.*, vol. 18, no. 3, pp. 173–175, Mar. 2008.

[41] M. Akra, E. Pistono, H. Issa, A. Jrad, and P. Ferrari, "Full study of the parallel-coupled stub-loaded resonator: synthesis method in a narrow band with an extended optimal rejection bandwidth," *IEEE Trans. Microw. Theory Techn.*, vol. 58, no. 12, pp. 3760–3769, Dec. 2010.

[42] S. Sun and L. Zhu, "Multiple-resonator-based bandpass filters," *IEEE Microw. Mag.*, vol. 10, no. 2, pp. 88–98, Apr. 2009.

[43] Z. C. Cheng and J.-S. Hong, "Ultrawideband filter technologies," *IEEE Microw. Mag.*, vol. 11, no. 4, pp. 56–68, Jun. 2010.

[44] A. R. Djordjevic and A. G. Zajic, "Low-reflection bandpass filters with a flat group delay," *IEEE Trans. Microw. Theory Techn.*, vol. 53, no. 4, pp. 1164–1167, Apr. 2005.

[45] B. W. Kim and S. W. Yun, "Varactor-tuned combline bandpass filter using step-impedance microstrip lines," *IEEE Trans. Microw. Theory Techn.*, vol. 52, no. 4, pp. 1279–1283, Apr. 2004.

[46] M. A. El-Tanani and G. M. Rebeiz, "Corrugated microstrip coupled lines for constant absolute bandwidth tunable filters," *IEEE Trans. Microw. Theory Techn.*, vol. 58, no. 4, pp. 956–963, Apr. 2010.

[47] W. Tang and J.-S. Hong, "Varactor-tuned dual-mode bandpass filters," *IEEE Trans. Microw. Theory Techn.*, vol. 58, no. 8, pp. 2213–2219, Aug. 2010.

[48] Y. C. Li and Q. Xue, "Tunable balanced bandpass filter with constant bandwidth and high common-mode suppression," *IEEE Trans. Microw. Theory Techn.*, vol. 59, no. 10, pp. 2452–2460, Oct. 2011.

[49] Q. Xiang, Q. Feng, X. Huang, and D. Jia, "Electrical tunable microstrip *LC* bandpass filters with constant bandwidth," *IEEE Trans. Microw. Theory Techn.*, vol. 61, no. 3, pp. 1124–1130, Mar. 2013.


**Roberto Gómez-García** (S'02–M'06–SM'11) was born in Madrid, Spain, in 1977. He received the Telecommunication Engineer and Ph.D. degrees in electrical and electronic engineering from the Polytechnic University of Madrid, Madrid, Spain, in 2001 and 2006, respectively.

Since April 2006, he has been an Associate Professor with the Department of Signal Theory and Communications, University of Alcalá, Alcalá de Henares, Madrid, Spain. His current research interests are the pursuit of new concepts to design fixed/tunable high-frequency filters and multiplexers in planar, hybrid, and monolithic microwave integrated circuit (MMIC) technologies, multi-function circuits, and novel software-defined radio and radar architectures for telecommunications, remote sensing, and biomedical applications.

Dr. Gómez-García is an associate editor for the IEEE TRANSACTIONS ON MICROWAVE THEORY AND TECHNIQUES, the IEEE TRANSACTIONS ON CIRCUITS AND SYSTEMS—I: REGULAR PAPERS, and *IET Microwaves, Antennas and Propagation*. He was a guest editor for the IEEE JOURNAL ON EMERGING AND SELECTED TOPICS IN CIRCUITS AND SYSTEMS 2013 "Special Issue on Advanced Circuits and Systems for CR/SDR Applications," the *IET Microwaves, Antennas and Propagation* 2013 "Special Issue on Advanced Tunable/Reconfigurable and Multi-Function RF/Microwave Filtering Devices," and the *IEEE Microwave Magazine* 2014 "Focused Issue on Recent Trends on RF/Microwave Tunable Filter Design." He is a member of the IEEE MTT-S Filters and Passive Components (MTT-8), IEEE MTT-S Biological Effect and Medical Application of RF and Microwave (MTT-10), IEEE MTT-S Wireless Communications (MTT-20), and IEEE CAS-S Analog Signal Processing Technical Committees.

**Andrew C. Guyette** (M'08) was born in Grand Forks, ND, USA, in 1976. He received the B.S. and M.S. degrees in electrical engineering from the University of Hawaii at Manoa, Honolulu, HI, in 1999 and 2001, respectively, and the Ph.D. degree from The University of Leeds, Leeds, U.K., in 2006.

Since 2007, he has been with the Naval Research Laboratory, Washington, DC, USA. His research interests include tunable filters, lossy filters, and network synthesis.